Research in Astron. Astrophys. **2010** Vol. **10** No. **1**, 83 – 90
http://www.raa-journal.org *http://www.iop.org/journals/raa*

***R**esearch in*
***A**stronomy and*
***A**strophysics*

Synthetic analysis of a two-ribbon microflare *

Cheng Fang, Peng-Fei Chen, Rong-Lin Jiang and Yu-Hua Tang

Department of Astronomy, Nanjing University, Nanjing 210093, China; *fangc@nju.edu.cn*

Received 2009 August 28; accepted 2009 September 25

Abstract High-resolution Stokes spectral data of Hα, Ca II 8542 Å, and Fe I 6302.5 Å lines for a two-ribbon microflare (TRMF) were simultaneously obtained by the THEMIS telescope on 2002 September 5. We derive the intensity, velocity, and longitudinal magnetic field maps. The hard X-ray emission observed by *RHESSI* provides evidence of nonthermal particle acceleration in the TRMF. Using Hα and Ca II 8542 Å line profiles and a non-LTE calculation, we obtain semi-empirical atmospheric models for the two brightest kernels of the TRMF. Our result indicates that the temperature enhancement in the chromosphere is more than 2500 K. The kinetic and radiative energies at the kernels are also estimated, resulting in an estimate of the total energy of the TRMF of about 2.4 $\times 10^{29}$ erg. Observations indicate that the TRMF results from the low coronal magnetic reconnection following the eruption of a small filament. However, the local temperature "bump" in the chromosphere presents a puzzle for such a standard flare model. A possible solution to this is discussed.

Key words: Sun: chromosphere — Sun: flares — Sun: activity — Sun: magnetic fields

1 INTRODUCTION

Microflares have been observed and studied for many years (e.g., Svestka 1976; Tandberg-Hanssen & Emslie 1988; Liu et al. 2004; Fang et al. 2006a). The typical size of microflares is several to 20 arcseconds, with a typical lifetime being 10–30 min and a total energy about $10^{26} - 10^{29}$ erg (e.g., Shimizu et al. 2002; Fang et al. 2006a). Microflares can appear not only in the lower solar atmosphere, but also in the transition region and corona, such as EUV (Emslie & Noyes 1978; Porter et al. 1984, 1987) and X-ray bright points (Lin et al. 1984; Krucker et al. 2002; Benz & Grigis 2002). Some observational results indicate that the emissions at different wavelengths are coincident. For instance, using the data of *Yohkoh*/SXT, *SOHO*/EIT and *TRACE*, Berghmans et al. (2001) found that the strongest EUV brightenings were the counterparts of soft X-ray microflares. Liu et al. (2004) studied 12 microflares with BBSO/Hα, *RHESSI* images at 3 to 15 keV, and *GOES* data, and found that all of them are observed in soft X-ray, hard X-ray and Hα. However, the physical relationship between them is still not clear and needs to be studied further. The most obvious characteristic in the visible spectra of chromospheric microflares is the weak emission at the center of the Hα line. This implies that there should be heating in the solar chromosphere. Semi-empirical models of chromospheric microflares indicate that the temperature enhancement is about 1000 – 2200 K (Fang et al. 2006a).

* Supported by the National Natural Science Foundation of China.

Observations indicate that mass motions exist at or close to the locations of chromospheric microflares. For instance, Shimizu et al. (2002) found that chromospheric ejections were observed in some microflares. Nonthermal properties of some microflares are explored by using microwave observations (e.g. Gary & Zirin 1988; White et al. 1995; Nindos et al. 1999) and hard X-ray emissions (e.g. Nitta 1997; Krucker et al. 2002; Liu et al. 2004; Qiu et al. 2004). It is also found that some microflares are located around magnetic polarity inversion lines (Porter et al. 1987; Shimizu et al. 2002; Liu et al. 2004; Fang et al. 2006a). Moreover, observational results show that in many cases the emerging flux occurs about 5 – 30 min before the microflares (e.g. Tang et al. 2000; Shimizu et al. 2002). Recently, Hinode observations show the ubiquitous presence of chromospheric anemone jets outside sunspots in active regions (Shibata et al. 2007). Some of them are probably related to chromospheric microflares. All these observations imply that magnetic reconnection in the chromosphere could be a plausible mechanism for chromospheric microflares.

A C1.6 two-ribbon microflare (TRMF) was observed on 2002 September 5 by THEMIS, a French–Italian 90 cm vacuum solar telescope at the Canary islands. High-resolution Stokes spectral data of Hα, Ca II 8542 Å, and Fe I 6302.5 Å lines for the TRMF were simultaneously recorded. Xia et al. (2007) analyzed the spectra of one kernel of this microflare. Their result indicates that magnetic reconnection and acceleration of particles mainly took place at the outer edges of the microflare ribbons. In this paper, we analyze the spectra of the brightest kernels and calculate their empirical atmospheric models in order to investigate how the heating of the microflare can be explained in terms of magnetic reconnection. The paper is organized as follows. The observation and data analysis are described in Section 2, the trigger mechanism of the TRMF is discussed in Section 3, and the discussion and a summary are given in Section 4.

2 OBSERVATIONS AND DATA ANALYSIS

2.1 Observations

A TRMF in the active region 10096 (S16E09) was observed on 2002 September 5 from 08:01 UT to 08:44 UT with THEMIS in the MTR multi-line spectropolarimetric mode (*http://www.themis.iac.es*). In this mode, the top part of the camera sequentially received $I+Q$, $I+U$, $I+V$, and $I-V$, while the bottom part recorded $I-Q$, $I-U$, $I-V$, and $I+V$. Three cameras simultaneously recorded the Stokes parameters for Hα, Ca II 8542 Å, and Fe I 6302.5 Å lines. After dark current and flat field corrections, the Muller matrix was used to demodulate the Stokes parameters. To remove the induced cross-talk and improve the seeing smearing, the two spectra are aligned well in the slit direction (the vertical direction), and then the top and bottom spectra are summed.

The TRMF was scanned with 80 steps within 2.5 min, covering $80''$ in the scanning direction. The spatial sampling along the slit is $0.42''$ pixel^{-1}. The spectral sampling is 26.1 mÅ for Hα, 36.3 mÅ for Ca II 8542 Å, and 22.4 mÅ for Fe I 6302.5 Å per pixel. The seeing condition was better than $1''$, but the scanning limited the spatial resolution to $\sim 2''$ for all 2D maps.

Using the bisector method for the Hα line profiles and Ca II 8542 Å Stokes-V profiles, we obtained the line-of-sight velocity field $v_{\parallel}$ and the longitudinal magnetic field $B_{\parallel}$, respectively (Xia et al. 2007). Figure 1 gives the $B_{\parallel}$ map (contour lines) overlaid on the Hα-center image at 08:12 UT, where the two crosses indicate the locations of the two bright kernels K1 (south) and K2 (north) of the TRMF. It can be seen that the longitudinal magnetic neutral line is located just between the two ribbons. The *Reuven Ramaty High-Energy Solar Spectroscopic Imager* (*RHESSI*) also detected the TRMF in the energy bands of 3−12 keV and 12−25 keV (see fig. 2 in Xia et al. 2007).

Using *RHESSI* data, we obtained an HXR image and the power law index of the TRMF. Figure 2 shows the results. It is seen that the microflare has significant HXR emissions, which present a very soft energy spectrum, with a power index of 8.1 and a flux of about 10^{10} erg s^{-1} cm^{-2} above 10 keV. According to the thick-target model, this implies that the energy spectrum of the nonthermal electrons has a power index of 9.1. It is interesting to note that the HXR emission in the higher

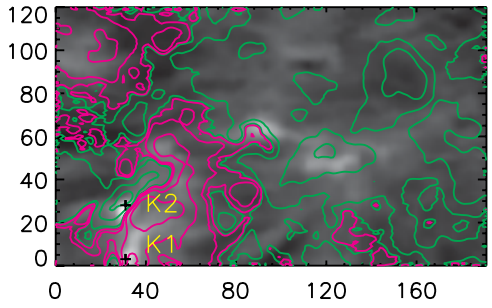

Fig. 1 $B_{\|}$ map (*contour*) overlaid on the Hα-center image (*grey*) of the TRMF at 08:12 UT. The crosses indicate the locations of the bright kernels K1 and K2 of the TRMF. The contour levels of the $B_{\|}$ are –800, –300, –50, –5, 4, 40, 200, and 500 G. The green and purple lines correspond to negative and positive polarity, respectively. The units of the coordinates are pixels, corresponding to $0.42''$.

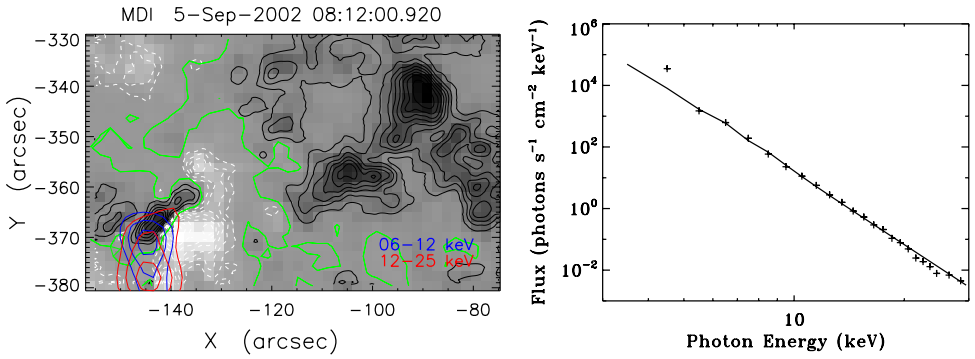

Fig. 2 HXR emission (*contour*) is overlaid on the $B_{\|}$ map (*gray, left*), where the green line is the longitudinal neutral line. The contour levels of the HXR emission are 50, 70, and 90 percent of the peak value. The power law fit of the HXR emission of the TRMF is also given (*right*).

energy band (12−25 keV) is concentrated at the kernel K1 where the magnetic field is weaker. This is consistent with the results for many flares (e.g., Sakao 1994).

2.2 Semi-empirical Atmospheric Model of the TRMF

Using the observed Hα and Ca II 8542 Å line profiles and non-LTE theory, we computed semi-empirical atmospheric models for the brightest kernels of the TRMF. The method of the non-LTE computation is similar to that given by Fang et al. (1993). Figure 3 gives the temperature distributions of the semi-empirical models. Figure 4 depicts the comparison between the computed and observed line profiles of the K2 kernel shown in Figure 1. It can be seen that the computation reproduces the observed spectral profiles for both lines well. Our semi-empirical atmospheric models indicate that there is an obvious temperature "bump" in the chromosphere. Compared to the quiet-

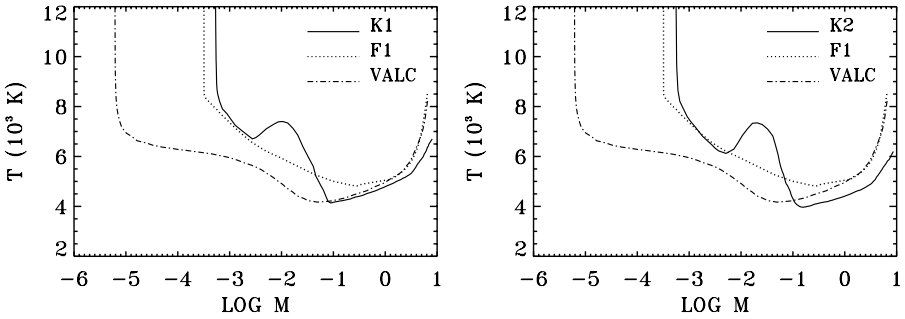

Fig. 3 Temperature distributions of the semi-empirical models for the bright kernels K1 (*left*) and K2 (*right*) of the TRMF (*solid lines*), compared with that of the flare model F1 (*dotted lines*) given by Machado et al. (1980), and the quiet-Sun atmospheric model VALC (*dash-dotted lines*) given by Vernazza et al. (1981).

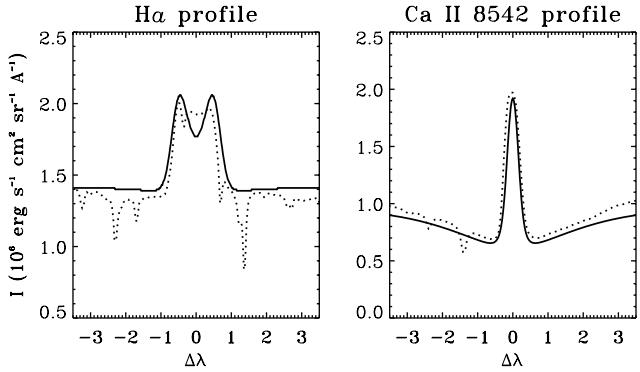

Fig. 4 Comparison between the observed (*dotted lines*) and computed (*solid lines*) Hα (*left*) and Ca II 8542 Å (*right*) line profiles of the K2 kernel. A Gaussian microturbulence velocity of 5 km s^{-1} is adopted to convolve the computed line profiles.

Sun atmospheric model (VALC), the maximum temperature enhancement in the chromosphere is about 2500 K.

Using the theory and the formula of the nonthermal collisional excitation and ionization rates of hydrogen and calcium given by Fang et al. (1993) and Hénoux et al. (1995), we perform computations of the nonthermal semi-empirical models for the kernels. In the computations, we use 9.1 as the power index of the electron beam and a flux of 10^{10} erg s^{-1} cm^{-2} above 10 keV, as deduced from the *RHESSI* HXR observation. The result indicates that the nonthermal effect is negligible in the heating of the TRMF. The reason for this is that the energy spectrum of the electron beam is so soft that the nonthermal electrons contribute little to the heating of the high-density chromosphere.

2.3 Energetics of the TRMF

Using our method given in Fang et al. (2006a) and the semi-empirical atmospheric models of the kernels, we can estimate the energy of the TRMF. The method is briefly described as follows.

Considering that the main heating regions are in the chromosphere, we use the radiative loss to evaluate the radiative energy $E_{\rm r}$:

$$E_{\rm r} = \frac{D}{2} S_{\rm k} \int_{h_1}^{h_2} R_{\rm r}\, dh \ , \tag{1}$$

where D, the lifetime of the TRMF, is taken to be 40 min (the heating duration is assumed to be D/2), $S_{\rm k}$ is the area of the K1 or K2 kernels, which is about $4''$ in diameter as evaluated by the kernel size on the Hα map, h_1 and h_2 are the lower and upper heights of the TRMF temperature-enhanced region, and $R_{\rm r}$ is the non-LTE radiative losses in units of erg cm^{-3} s^{-1}. We modified the empirical formula given by Gan & Fang (1990) to make it more suitable for small activities such as microflares. Our modified formula is as follows (Jiang et al. 2009):

$$R_{\rm r} = n_{\rm H} n_{\rm e} \alpha(y) f(T), \tag{2}$$

where $\alpha(y)$ and $f(T)$ are functions of y (i.e., the height from $\tau_{5000} = 1$ in the photosphere) and the temperature T respectively, and defined as follows:
$\alpha(y) = 10^{(1.745\times10^{-3}y - 4.739)} + 8.0\times10^{-2} e^{-3.701\times10^{-2}y}$,
$f(T) = 4.533\times10^{-23}(\frac{T}{10^4})^{2.874}$,
where the unit of y is km. Then the net radiative energy of the kernel can be evaluated by

$$\Delta E = E_{\rm r} - E_{\rm Q} \ , \tag{3}$$

where $E_{\rm Q} = \frac{D}{2} S_k \int R_{\rm Q} dh$ is the total radiative loss of the quiet-Sun atmospheric model VALC (Vernazza et al. 1981), in which $\int R_{\rm Q} dh$ = 4.6$\times10^6$ erg cm^{-2} s^{-1}. In fact, our results indicate that $E_{\rm Q}$ is about one or two orders of magnitude smaller than $E_{\rm r}$.

By use of the line-of-sight velocity measurement near the kernel, the lower limit of the kinetic energy can be estimated as

$$E_v = \frac{1}{2} 1.4 m_{\rm H} v_{\parallel}^2 f S_k \int_{h_3}^{h_4} n_{\rm H} dh \ , \tag{4}$$

where $n_{\rm H}$ is the hydrogen density in the heating region of the kernel and f is the fraction of the mass that is involved in motion. We assume that f = 0.1, because it seems that the heated plasma cannot be fully ejected during the magnetic reconnection. In this case, h_3 and h_4 are the lower and upper heights of the heated kernels, respectively, which are determined according to the semi-empirical model of the kernels. The measured line-of-sight velocity $v_\parallel$ is about 2 km s^{-1} for both the K1 and K2 kernels.

By use of the formulae (3) and (4), the energies of the two kernels of the TRMF can be estimated, and are listed in Table 1. It can be seen that the total energy at K1 is a little higher than that at K2. This may be related to the fact that the HXR emission at K1 is harder that that at K2 (see Fig. 2). Considering that the size of each ribbon is about $14''\times5''$, and assuming that on average the energy in other regions of the ribbon is four times smaller than that of the kernels, we estimate the total energy of the TRMF to be 2.4 $\times10^{30}$ erg, which is more than one order of magnitude larger than that of the bright microflares we have studied (Fang et al. 2006a).

Table 1 Parameters Used to Estimate the Energy of the Two Kernels

Kernel	h_1 (km)	h_2 (km)	h_3 (km)	h_4 (km)	$v_\parallel$ (km s^{-1})	ΔE (erg)	E_v (erg)
K1	260	1380	480	1030	2.0	9.9 $\times10^{28}$	6.4 $\times10^{26}$
K2	240	1420	440	1026	2.0	6.4 $\times10^{28}$	7.3 $\times10^{26}$

3 TRIGGER MECHANISM OF THE TRMF

It can be seen that the TRMF has some typical characteristics of the usual two ribbon flares: an obvious two-ribbon-like structure in its Hα image indicating heating in the chromosphere, two bright kernels located on two sides of the longitudinal magnetic neutral line, HXR emissions with a power-law spectrum, etc. It is generally recognized that an ordinary two-ribbon flare can be triggered by a filament eruption. We do find evidence showing a possible small filament eruption before the TRMF. Using the bisector method, we obtained the line-of-sight velocity distribution, which is shown in Figure 5 for 08:01 UT (left) and 08:12 UT (right), respectively.

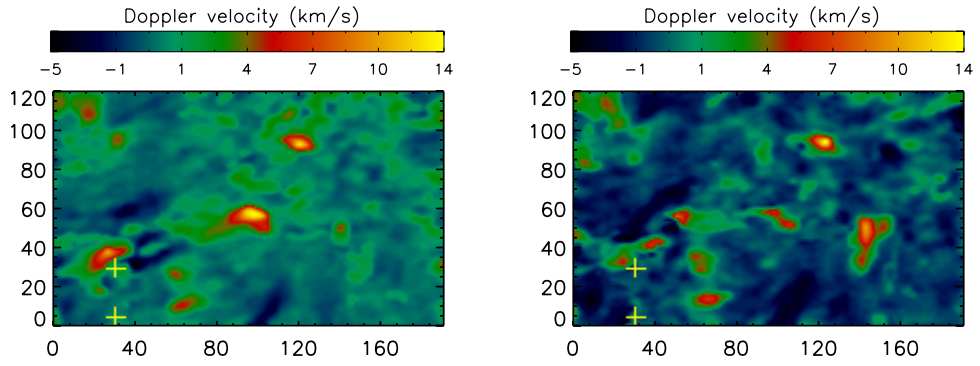

Fig. 5 Line-of-sight velocity distributions of the TRMF at 08:01 UT (*left*) and 08:12 UT (*right*). Negative and positive velocities correspond to upflow and downflow, respectively. The crosses indicate the locations of the bright kernels K1 (*lower*) and K2 (*upper*) of the TRMF. The units of the coordinates are pixels, corresponding to 0.42″.

It can be clearly seen that just before the TRMF, at 08:01 UT near the K2 kernel, there was a small filament eruption with an upward velocity of about several km s $^{-1}$, which is much lower than the typical velocity of the erupting filament for ordinary large two-ribbon flares. At 08:12 UT, the rising filament almost disappeared.

4 DISCUSSION AND SUMMARY

Most microflares are located near longitudinal magnetic neutral lines, often accompanied by mass motions. Semi-empirical models always indicate that there exists a local temperature enhancement in the chromosphere which is about 2500 K. All these, together with some theoretical work, imply that magnetic reconnection in the lower solar atmosphere is responsible for microflares (e.g., Tandberg-Hanssen & Emslie 1988; Liu et al. 2004; Fang et al. 2006a), as well as other small activities like Ellerman bombs (e.g., Fang et al. 2006b; Ding et al. 1998; Chen et al. 2001; Watanabe et al. 2008), which are chromospheric in nature.

For the TRMF studied here, the semi-empirical models also indicate that there is a temperature "bump" located at a height $\sim 800 - 1000$ km in the chromosphere. However, the observations also show evidence that the TRMF is triggered by the eruption of a small filament above the magnetic neutral line. The distance between the two ribbons measured in the Hα image (see Fig. 1) is about 10″, corresponding to $\sim 7000 - 8000$ km. We can then estimate that the height of the X-point, where magnetic reconnection occurs, is about 10^4 km above the photosphere. That is to say, the magnetic reconnection is located in the low corona. This leads to a question: how can the energy released

by the low coronal magnetic reconnection be transferred into the chromosphere and produce the localized temperature "bump?" Heat conduction does not seem to be applicable since it would heat the chromosphere all the way through. Radiative back-warming is also not important, because the TRMF is only a small flare. Moreover, as pointed out in Section 2.3, our calculation also indicates that the nonthermal effect is negligible for the heating of the TRMF, if we use an electron beam power index of 9.1 and a flux of 10^{10} erg s^{-1} cm^{-2} above 10 keV as deduced from the *RHESSI* HXR observation. Therefore, the existence of a localized temperature "bump" presents a severe puzzle.

One possibility might be that the nonthermal energy spectrum obtained from the *RHESSI* observations is in fact softer than the real one since the hard X-rays experience Compton scattering on their way through the chromosphere (see, e.g., Suleimanov & Werner 2007). Such an effect has been neglected before, which might result in a softer energy spectrum for the nonthermal electrons. The real energy spectrum of nonthermal electrons bombarding the chromosphere may be harder than that obtained with the widely-used model. In this case, the power index of the electron beam produced in the magnetic reconnection might be harder, so that the electron beam can easily penetrate into the chromosphere and deposit the energy in a localized region of the chromosphere, causing the temperature "bump." Such an issue is worth studying in the future.

As a summary, we give the following conclusions:

1. Using non-LTE theory and the observed high-resolution Stokes spectral data of Hα, Ca II 8542 Å, and Fe I 6302.5 Å lines, we obtained the semi-empirical atmospheric models for the two brightest kernels of a TRMF. Our result indicates that the temperature enhancement in the chromosphere is more than 2500 K and the total energy of the TRMF is about 2.4×10^{29} erg.
2. The TRMF is triggered by the eruption of a small filament followed by magnetic reconnection appearing in the low corona. However, the cause of the temperature "bump" in the chromosphere is still not clear. We tentatively propose that it is produced by nonthermal electrons. If so, it is suggested that Compton scatterring of the hard X-rays in the chromosphere, which has often not been considered in deducing the energy spectrum for nonthermal particles, may not be neglected.

Acknowledgements We would like to thank Mr. Q. R. Chen, who kindly provided valuable help in analyzing the *RHESSI* data. This work was supported by the National Natural Science Foundation of China (NSFC) (Grant Nos. 10221001, 10878002, 10403003, 10620150099, 10610099, 10933003 and 10673004), as well as a grant from the 973 project 2006CB806302.

References

Benz, A. O., & Grigis, P. C. 2002, Solar Phys., 210, 431
Berghmans, D., McKenzie, D., & Clette, F. 2001, A&A, 369, 291
Chen, P. F., Fang, C., & Ding, M. D. 2001, ChJAA (Chin. J. Astron. Astrophys.), 1, 176
Ding, M. D., Hénoux, J. C., & Fang, C. 1998, A&A, 332, 761
Emslie, A. G., & Noyes, R. W. 1978, Solar Phys., 57, 373
Fang, C., Hénoux, J. C., & Gan, W. Q. 1993, A&A, 274, 917
Fang, C., Tang, Y. H., & Xu, Z. 2006a, ChJAA (Chin. J. Astron. Astrophys.), 6, 597
Fang, C., Tang, Y. H., Ding, M. D., & Chen, P. F. 2006b, ApJ, 643, 1325
Gary, D. E., & Zirin, H. 1988, ApJ, 329, 991
Gan, W. Q., & Fang, C. 1990, ApJ, 358, 328
Hénoux, J. C., Fang, C., & Gan, W. Q. 1995, A&A, 297, 574
Jiang, R. L., Fang, C., & Chen, P. F. 2009, to be submitted
Krucker, S., Christe, S., Lin, R. P., et al. 2002, Solar Phys., 210, 445
Lin, R. P., Schwartz, R. A., Kane, S. R., et al. 1984, ApJ, 283, 421

Liu, C., Qiu, J., Gary, D. E., et al. 2004, ApJ, 604, 442
Machado, M. E., Avrett, E. H., Vernazza, J. E., et al. 1980, ApJ, 242, 336
Nindos, A., Kundu, M. R., & White, S. M. 1999, ApJ, 513, 983
Nitta, N. 1997, ApJ, 491, 402
Porter, J. G., Toomre, J., & Gebbie, K. B. 1984, ApJ, 283, 879
Porter, J. G., Moore, R. J., Reichmann, E. J., et al. 1987, ApJ, 323, 380
Qiu, J., Liu, C., Gary, D. E., et al. 2004, ApJ, 612, 530
Sakao, T. 1994, Ph.D. thesis, University of Tokyo
Shibata, K., Nakamura, T., Matsumoto, T., et al. 2007, Science, 318, 1591
Shimizu, T., Shine, R. A., Title, A. M., et al. 2002, ApJ, 574, 1074
Suleimanov, V., & Werner, K. 2007, A&A, 466, 661
Svestka, Z. 1976, Solar Flares (Dordrecht: D. Reidel Publ. Co., Holland)
Tang, Y. H., Li, Y. N., Fang, C., et al. 2000, ApJ, 534, 482
Tandberg-Hanssen, E., & Emslie, A. G. 1988, The Physics of Solar Flares (Cambridge: Cambridge Univ. Press)
Vernazza, J. E., Avrett, E. H., & Loeser, R. 1981, ApJS, 45, 635
Watanabe, H., Kitai, R., Okamoto, K., et al. 2008, ApJ, 684, 736
White, S. M., Kundu, M. R., Shimizu, T., et al. 1995, ApJ, 450, 435
Xia, C., Fang, C., Chen, Q. R., & Tang, Y. H. 2007, Adv. Space Res., 39, 1402